Inorganic Chemistry

Generalized Stress-Redox Equivalence: A Chemical Link between Pressure and Electronegativity in Inorganic Crystals

Álvaro Lobato,[†,‡] Hussien H. Osman,[*,†,§] Miguel A. Salvadó,[†] Pilar Pertierra,[†] Ángel Vegas,[⊥] Valentín G. Baonza,[‡,∥] and J. Manuel Recio[*,†]

[†]MALTA-Consolider Team and Departamento de Química Física y Analítica, Universidad de Oviedo, E-33006 Oviedo, Spain

[‡]Malta-Consolider Team and Departamento de Química Física, Universidad Complutense de Madrid, E-28040 Madrid, Spain

[§]Department of Chemistry, Faculty of Science, Helwan University, Ain-Helwan, 11795 Cairo, Egypt

[⊥]University of Burgos, Hospital del Rey, E-09001 Burgos, Spain

[∥]Instituto de Geociencias IGEO, CSIC-UCM, E-28040 Madrid, Spain

S *Supporting Information*

ABSTRACT: The crystal structure of many inorganic compounds can be understood as a metallic matrix playing the role of a host lattice in which the nonmetallic atomic constituents are located, the Anions in Metallic Matrices (AMM) model stated. The power and utility of this model lie in its capacity to anticipate the actual positions of the guest atoms in inorganic crystals using only the information known from the metal lattice structure. As a pertinent test-bed for the AMM model, we choose a set of common metallic phases along with other nonconventional or more complex structures

(face-centered cubic (fcc) and simple cubic Ca, CsCl-type BaSn, hP4-K, and fcc-Na) and perform density functional theory electronic structure calculations. Our topological analysis of the chemical pressure (CP) scalar field, easily derived from these standard first-principles electronic computations, reveals that CP minima appear just at the precise positions of the nonmetallic elements in typical inorganic crystals presenting the above metallic subarrays: CaF_2, rock-salt, and CsCl-type phases of CaX (X = O, S, Se, Te), $BaSnO_3$, K_2S, and NaX (X = F, Cl, Br, I). A theoretical basis for this correlation is provided by exploring the equivalence between hydrostatic pressure and the oxidation (or reduction) effect induced by the nonmetallic element on the metal structure. Indeed, our CP analysis leads us to propose a generalized stress-redox equivalence that is able to account for the two main observed phenomena in solid inorganic compounds upon crystal formation: (i) the expansion or contraction experienced by the metal structure after hosting the nonmetallic element while its topology is maintained and (ii) the increasing or decreasing of the effective charge associated with the anions in inorganic compounds with respect to the charge already present in the interstices of the *metal network*. We demonstrate that a rational explanation of this rich behavior is provided by means of Pearson-Parr's electronegativity equalization principle.
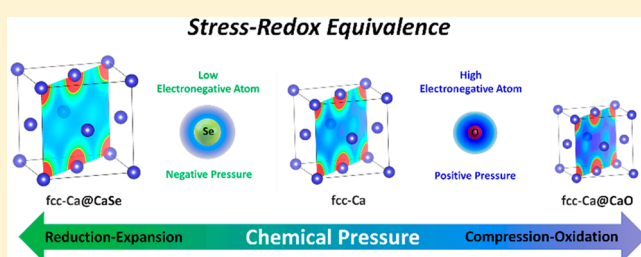
1. INTRODUCTION

The literature on the theories and formalisms describing chemical bonding in inorganic crystal structures is very extensive,[1−6] and the models can typically be classified into either classical or quantum types. Among them, the approach of Pauling has been the paradigm for describing and rationalizing the crystal structures of ionic compounds over the last century.[7,8] The limitations of the ionic model, which have also led to a number of misconceptions about the crystal structure and the bonding network, were discussed by O'Keeffe and Hyde using alternative approaches.[9,10] These authors put the emphasis on the description of the structures of oxides as oxygen-stuffed alloys, since their cationic sublattices adopt the structures of either elements or simple alloys. Interestingly, this concept can also be applied to the naked metallic structure if the valence electrons localized in the empty spaces of the structure are conceived as *coreless*

pseudoanions. In fact, the term electride was introduced after an extensive quantum-mechanical treatment of a high-pressure modification of metallic cesium that led to denote this phase as Cs+e−.[11] Prior to these calculations, Schubert already proposed that the valence electrons might be well-located at the voids of the metals/alloys structures.[12] This idea was also applied by Vegas et al. in a more recent work.[13]

The consideration of the metallic matrix of a compound as a host lattice for nonmetallic atoms was indeed formalized later by Vegas et al.[14−16] in the so-called anions in metallic matrices (AMM) model. According to the AMM model, the electronic structure and the atomic arrangement of the metallic sublattice induce the equilibrium positions of the nonmetallic atoms in the crystal. This idea culminated a wide variety of studies that

63 take into account not only a dense packing of atoms, as in
64 metals and/or alloys, but also more open metal skeletons such
65 as those present in AlX_3 structures (X = F, Cl, OH).[15] The
66 AMM model found support from several theoretical
67 calculations in a variety of systems including the AlX_3 crystals,
68 boron phosphide in the zinc blende phase, and high-pressure
69 phases of Na and K, to cite a few.[16−18] Topological analyses of
70 the electron density of these structures reveal that the valence
71 electrons of the metal are found to be localized in interstitial
72 positions, where anions are found in inorganic compounds, or
73 close to the sites of bonding and lone electron pairs. These
74 electronic domains were named pseudoanions and preceded
75 the concept of Interstitial Quantum-Atoms later introduced by
76 Miao and Hoffmann.[19,20] In other examples (face centered
77 cubic (fcc) and simple cubic (sc) phases of Ca), the topology
78 of the electron localization function (ELF) was also evaluated
79 to reveal the correlation between the interstitial positions of
80 ELF attractors in the corresponding unit cells and the positions
81 of the oxygen atoms in the rock-salt and CsCl-type phases of
82 CaO.[21] The same result is obtained when the ELF topology in
83 the high-pressure CsCl-type phase of BaSn alloy is evaluated to
84 anticipate the preferential positions of oxygen in the perovskite
85 $BaSnO_3$.[21] In all these cases, the topological evidence appears
86 and/or is enhanced when the metal is explored in the actual
87 strained configuration presented at the equilibrium structure of
88 the inorganic crystal. The enhanced effect induced by the
89 nonmetallic atom is an inherent feature of the AMM model
90 that corresponds to the concept of pressure-oxidation
91 equivalence and requires further exploration.[22]

92 This equivalence between chemical oxidation and external
93 macroscopic pressure was proposed by Martínez-Cruz et al.[23]
94 and more exhaustively illustrated for a large set of compounds
95 by Vegas and Jansen.[14,22] Cations are not independent
96 chemical entities filling voids in the corresponding anionic
97 subarrays as usually described by the ionic model. They are
98 instead arranged keeping the same lattice structure as in the
99 *isolated* metals but showing strained unit cells induced by the
100 embedding of nonmetallic atoms. If the effect of the
101 nonmetallic atom is strong enough, the metallic sublattice in
102 the inorganic crystal may display a structure not stable at its
103 equilibrium conditions but another one among those present
104 in the metal/alloy phase diagram. To cite a couple of examples
105 that will be analyzed later in this work, the potassium sublattice
106 in K_2S is the hP4 phase found in metallic K at very high
107 pressure,[18] and BaSn alloy in $BaSnO_3$ presents the high-
108 pressure CsCl-type structure to which the CaSi-type zero
109 pressure structure transforms. The physical principle or
110 explanation behind this behavior has not been reported, to
111 the best of our knowledge.

112 Recently, a simple implementation of the quantum-
113 mechanical stress density formalism has been developed,[24−28]
114 the chemical pressure (CP) approach.[29] This new scheme
115 provides bonding patterns in which the various types of
116 interatomic interactions (ionic, covalent, metallic, H-bond,
117 dispersion) are clearly differentiated[30] and can also be used to
118 track the bond formation and rupture processes in crystalline
119 solids.[31] The CP method is now widely applied for analyzing
120 the atomic size effects and the corresponding interactions with
121 the surrounding atoms in the solid state.[32−35] For our
122 purposes, the exploration of two-dimensional (2D) and
123 three-dimensional (3D) CP maps in metals and inorganic
124 crystals is especially convenient, since those regions in the
125 maps with low chemical pressure are identified with unit cell

126 positions showing a preference for electron density accumu-
127 lation. In addition, since the CP field is not a scaled property
128 (as it happens, e.g., with the ELF), variations of CP values
129 either induced by hydrostatic pressure or by the presence of
130 other chemical elements provide useful information about the
131 observed correlation between these two effects that deserves
132 further investigation.

133 In this Article, our first goal is to examine whether or not the
134 CP formalism supports the AMM model. To this end we
135 choose a research test bed involving metal structures of
136 different complexity as the fcc- and sc-Ca, CsCl-type BaSn,
137 hP4-K, and fcc-Na lattices. Once the assessment of the AMM
138 model is verified, our next focus will be to explain why the
139 positions of the anions in a given inorganic crystal can be
140 anticipated just resorting to its subjacent metallic sublattice.
141 Plausible answers associate these positions to particular
142 topological features in the electron density, the ELF, or the
143 CP maps of the metallic structures. However, our challenge
144 here is to find an underlying justification to account for both
145 the positive and negative strains experienced by the metallic
146 sublattices as a result of the effect induced by the nonmetallic
147 guest elements. We show that atomic sizes do not necessarily
148 account for the observed distortions and that a more profound
149 explanation in terms of the host and guest capacity to attract/
150 donate electron density is needed. The goal will be
151 accomplished after proposing a generalized stress-redox
152 equivalence, which is further supported by Pearson-Parr's
153 electronegativity equalization principle.[36−38] In essence, by
154 modifying the size of the metallic lattice, the charge located at
155 the interstice positions changes in a way that correlates with
156 the electronegativity of the nonmetallic element occupying
157 those positions. This reasoning will be illustrated using density
158 functional theory (DFT) CP results on the metallic lattices
159 collected above and on a number of halide and chalcogenide
160 inorganic crystals containing these metallic arrays.

161 The Article is divided into four more sections plus a
162 Supporting Information file. Computational details of the
163 electronic structure calculations and the CP approach are
164 presented in the following section. In Section 3, the AMM
165 model is checked in the light of the DFT-CP approach using a
166 number of metal (alloy)/inorganic crystal couples. Section 4
167 contains the results of the new generalized stress-redox
168 correlation with a discussion guided by the electronegativity
169 equalization principle. The Paper ends with a summary of our
170 findings and the most relevant conclusions of our study. In the
171 Supporting Information file, we included some technical details
172 about the calculations together with the CP analysis of fcc- and
173 sc-Mg and the electronegativity-CP correlations for fcc-Mg and
174 fcc-Na. A brief description of the unit cell of the structures
175 discussed in the main text is also provided.

2. COMPUTATIONAL DETAILS

176 DFT-chemical pressure calculations were performed on the
177 pair systems Ca/CaO, BaSn/$BaSnO_3$, K/K_2S, and Na/NaX (X
178 = F, Cl, Br). The local density approximation (LDA)
179 exchange-correlation functional of Goedecker, Teter, and
180 Hutter[39] and Hartwigsen-Goedecker-Hutter norm-conserving
181 pseudopotentials[40] were used under the formalism of DFT as
182 implemented in the ABINIT software package.[41−43] The
183 semicore electrons of all the metals were included in the
184 calculations. The geometrical optimization of the unit cells was
185 performed with the Broyden-Fletcher-Goldfarb-Shanno mini-
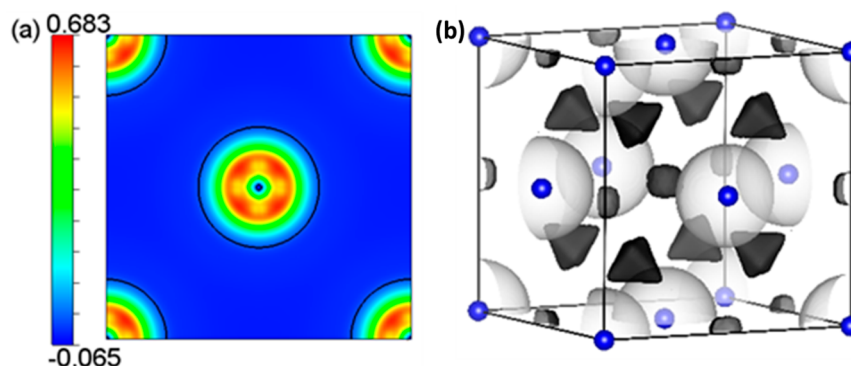186 mization algorithm. Further details regarding cutoff energies

Figure 1. CP analysis of fcc-Ca at equilibrium conditions. (a) Cross section along the (001) plane containing the Ca atoms. The CP = 0 contour is shown with a black solid line. (b) 3D isosurfaces with CP= +0.001 (white) and CP = −0.0274 (black). Pressures are given in atomic units.

and Monkhorst−Pack k-point[44] grids are collected in the Supporting Information file.

In the Chemical Pressure formalism, the total DFT energy of the system is expressed as an integral all over the space of the energy density (ρ_{energy}):

$$E_{\text{DFT}} = \int \rho_{\text{energy}} d\tau \tag{1}$$

In analogy to the thermodynamic macroscopic pressure, a microscopic chemical pressure (CP) is defined as the derivative of the local energy with respect to the volume, where the local energy ($\varepsilon_{\text{voxel}}$) is calculated in each of the small parallelepipeds (voxels) in which the 3D space is divided:

$$p_{\text{voxel}} = -\frac{\partial \varepsilon_{\text{voxel}}}{\partial v_{\text{voxel}}} \tag{2}$$

To perform such a derivative, we adopt the procedure proposed by Fredrickson in which the energy density (ρ_{energy}) is calculated in the real space, and then we perform numerically the derivative with respect to the volume. Further details are given elsewhere.[32−35,45] To apply the same scheme to all the systems reported in this work, three single-point calculations were always performed over a volume change of 0.5% around the corresponding equilibrium unit cell volumes using the Fredrickson group CP package.[29] In all the cases, the core unwarping method was used to reduce the strong features around the cores as explained in our previous works.[29,35]

The above computational details define the standard DFT-CP scheme followed in previous papers (see, e.g., refs 30 and 45 and refs therein). Nonetheless, we checked that differences are not meaningful when CP maps obtained with the standard procedure followed in this paper are compared with those obtained from generalized gradient approximation (GGA) calculations (computational details and maps are collected in the Supporting Information file). The CP maps were then rendered using the VESTA program.[46] Pressure values are given throughout the manuscript in atomic units unless otherwise specified (1 au = 29 421 GPa). Bader atomic charges[47] and electron density integrations in the positive pressure regions enclosed by CP = 0 contour isosurfaces were performed using Critic2 code[48] with the Yu−Trinkle integration method.[49]

3. ASSESMENT OF THE ANIONS IN METALLIC MATRICES MODEL

The basic premise of the AMM model states that the metallic arrangement and its electronic structure reveal the specific positions of the anions in the corresponding inorganic crystals.[50] In this section, we aim to illustrate whether the CP formalism is able or not to support the basis of the AMM model. Bearing in mind this idea, we selected several common metallic phases along with other nonconventional or more complex structures (fcc and sc-Ca, CsCl-BaSn, hP4-K, and fcc-Na), where nonmetallic elements such as chalcogenides and halides form typical inorganic crystals as CaF_2, CaX (X = O, S, Se, Te), $BaSnO_3$, K_2S, and NaX (X = F, Cl, Br, I). This selection constitutes a large enough number of examples going from stable zero pressure to high pressure phases, displaying different guest positions and allowing us to finally address the linking between the effect of mechanical pressure and chemical oxidation.

Let us start describing the main features emerging from the application of the CP formalism to the fcc structure of Ca. This is the stable phase of Ca at zero pressure and low temperature with a lattice parameter of a = 5.588 Å. Figure 1a shows the 2D CP map of the fcc-Ca unit cell in which intense positive CP features (red) around the nucleus reflect the semicore [$3s^2$ $3p^6$] electrons of the Ca atom. This positive CP gradually and radially decreases as we move from the nuclear position toward the neighboring atoms through a plateau region of negative CP (blue). In addition, each atomic position is surrounded by a contour line (black) of zero chemical pressure, which turns to be of a spherical shape in the 3D space and contains the atomic nucleus and the core electron pressure of the metallic atom. Such CP features are common to all results hereafter. This is in concordance with the so-called free electron model of metals.[51,52] According to the CP formalism,[30] positive values indicate that, in these regions, a decrease of the volume will increase the energy. Therefore, they are associated with repulsive regions, where the electron density tends to expand. In contrast, the negative CP background, representing the delocalized sea of valence electrons, is associated with the cohesion of the nuclei, because in these regions the electron density *looks for* a reduction of volume to decrease its energy as dictated by eq 2.

However, a closer analysis of the negative background reveals inhomogeneities in the local CP distribution that are crucial to validate the AMM model, as we will show in the ongoing discussion. By selecting appropriate negative and

positive values, with the purpose of representing regions enclosing CP minima and maxima, the 3D CP plot of fcc-Ca can be constructed (see Figure 1b). Two nonequivalent isosurfaces of negative (black) pressures clearly appears in the unit cell. One of those negative CP isosurfaces is located at the tetrahedral 8c sites (1, 1, 1), with a CP value of −0.0278 au, whereas the other appears at the 4b positions with a value of −0.0275 au. In agreement with the AMM model, these are exactly the coordinates where fluoride atoms in the archetypical fluorite structure and chalcogenide elements in the rock-salt structure are situated, respectively.

Indeed, equivalent features have been observed by the ELF analysis in fcc-Ca.[21] In their paper, Vegas and Mattessini revealed the presence of an ELF attractor at the (1/2, 1/2, 1/2) position, whereas in the case of the (1, 1, 1) position the situation was not so evident. In this regard, the CP formalism provides a neat picture for the potential guest positions in the fcc-Ca lattice. But what we would like to emphasize here is that the CP approach offers an extra insight about these preferential positions in the lattice informing when an accumulation of the electron density available for the anion formation is favored. For example, when pressure is applied to the fcc-Ca phase to achieve its volume in the rock-salt phase of CaO, the CP minima at the 8c and 4b positions decreases to −0.0422 and −0.0424 au, respectively. Such a decrease in the CP minima values can be attributed to an increase in the electron density accumulated through the interstitial positions. Although this feature will be discussed later, we want to remark that this behavior is a general result for the metallic phases and has a strong correlation with the rationalization of inorganic structures in the light of the AMM model.

To continue with the link between the CP formalism and the privileged positions for the anions in the metallic matrices, we applied the previous strategy to the simple cubic sc-Ca phase. This is one of the high-pressure phases found in the polymorphic sequence of metallic Ca (see, e.g., ref 53 for a thorough study of the experimental phase diagram of Ca). Indeed, the more open sc phase displays a valence band with a greater d-band character than the low-pressure structures, as discussed by Errandonea et al.[54] and Rahm et al.[55] Therefore, this is an excellent example to test if the proposed methodology can support the AMM model in a different scenario. At 39 GPa, sc-Ca presents a lattice parameter of 2.62 Å. In this structure, only one CP minimum appears in the unit cell at (1/2, 1/2, 1/2) suggesting this preferential position for the nonmetallic element. In fact, in the high-pressure CsCl phases of CaX (X = O, S, Se, Te) crystals, X^{2-} anions are situated at this same precise position identified by the CP formalism (see Figure 2).

Once we have considered simple examples of a pure metal, let us explore how the CP analysis performs in the binary BaSn alloy. At high pressure, BaSn transforms from the CaSi-type to the CsCl-type structure,[56] which can be considered as the metallic skeleton of the well-known $BaSnO_3$ perovskite. Successfully, the 3D CP isosurfaces of the CsCl-type structure of BaSn, calculated at the equilibrium volume of the perovskite $BaSnO_3$ phase (a = 4.1168 Å), display six regions enclosing CP minima at the centers of the faces of the cubic cell forming an octahedral environment around the Sn atom (see Figure 3). The positions of these localized regions of negative CP coincide with the coordinates where O atoms are located in the perovskite structure of $BaSnO_3$ in concordance also with the ELF topological analysis of Vegas and Mattessini.[21]
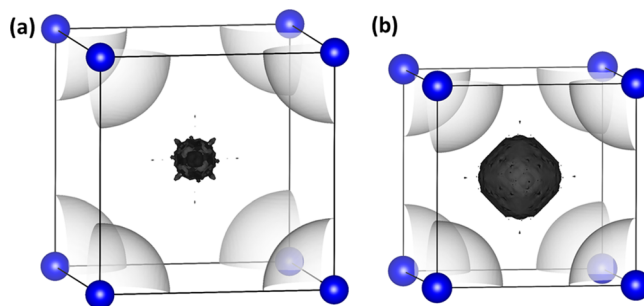

Figure 2. 3D CP isosurfaces of sc-Ca crystal at (a) the equilibrium volume with CP = +0.001 (white) and CP = −0.032 (black) and (b) the volume of the CsCl-CaO crystal with CP = +0.001 (white) and CP = −0.066 (black). Pressures are given in atomic units.
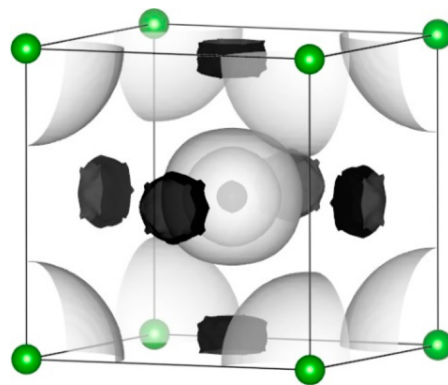

Figure 3. 3D CP isosurfaces of BaSn lattice (Ba = green, Sn = blue) at the equilibrium volume of $BaSnO_3$. White and black isosurfaces are of CP = +0.001 and CP = −0.0125 au, respectively.

In the same way, metallic K adopts an hP4 phase at very high pressure analogous to the K-substructure of the Ni_2In-type phase of K_2S obtained under pressure.[57] This K phase has been extensively studied, since Marqués et al.[18] demonstrated that the topologies of the electron density and the ELF show local attractors at the unoccupied 2d (1/3, 2/3, 3/4) positions leading to the consideration of this K phase as an electride. Showing the preference for these positions by means of the CP analysis is challenging given the low symmetry and the extreme conditions needed for the stabilization of this structure. Our CP results of the hP4-K phase show negative CP regions centered at the same positions where electrons in the electride and anions in the Ni_2In-type structures of several dialkali-metal monochalcogenides such as Na_2S, Rb_2Te and K_2SO_4 are found (see Figure 4).

We now turn to the fcc structure of Na to complete our CP analysis of metallic lattices. Although body-centered cubic (bcc) Na is the stable phase at room conditions, the fcc structure is the one present in the low-pressure rock-salt phases of NaX crystals (X = F, Cl, Br). Our expectation from the CP analysis of these fcc-Na lattices at the different equilibrium dimensions of the corresponding halides would be at least the presence of negative CP regions at the 4b (1/2, 1/2, 1/2) positions, since these are the coordinates of the X halides in their rock-salt phase. In fact, these positions clearly appear in the 3D CP representations shown in Figure 5. In addition, as in the first example discussed in this section (fcc-Ca), eight minima also appear at the (1, 1, 1) coordinates. We propose that these positions are potential sites for a hypothetical anion, although the stoichiometry requires a fractional negative
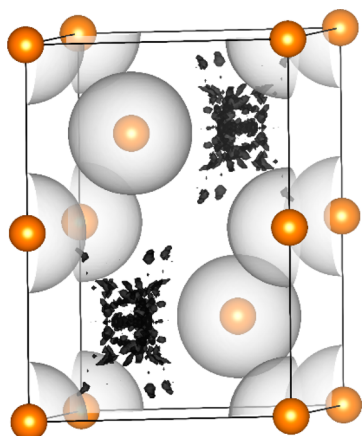
Figure 4. 3D CP isosurfaces in the hP4 phase of metallic K at the volume of K_2S compound. White and black isosurfaces are of CP = +0.001 and CP = −0.043 au, respectively.

charge of −0.5e given the multiplicity of this position. Nevertheless, evidence of the preference of electrophilic entities for this position are provided when examining the minimum energy diffusion path of negative defects, which go through this position.[58,59] It is interesting to notice that the same qualitative view is obtained regardless of the dimensions of the unit cell. The global analysis of the CP maps of the metallic sublattices of NaF, NaCl, and NaBr gives the following values for the black isosurfaces located at the expected 4b (1/2, 1/2, 1/2) positions of the anions: −0.0443, −0.0212, and −0.0172 au for NaF (2.31 Å), NaCl (2.56 Å), and NaBr (2.64 Å), respectively, while the CP minima at the 8c sites (1, 1, 1) are −0.0439, −0.0210, and −0.0170 au for the same latter crystals. Such a trend in the CP values points toward a relationship between the nature of the anion and the size of the metallic unit cell, supporting not only the AMM model but also pointing to the connection between oxidation and pressure that we will examine in the following section.

To sum up, through this section of the paper we carefully depicted the CP description of a number of metallic structures. Our results clearly demonstrate that CP minima reveal positions in the unit cell totally consistent with those that occupy nonmetallic elements in the inorganic compounds. Moreover, in addition to the ideas previously derived by the electron density and ELF analysis, CP provides a direct support to the AMM model in terms of energetic considerations and electron density accumulations that will be disclosed in the next section.
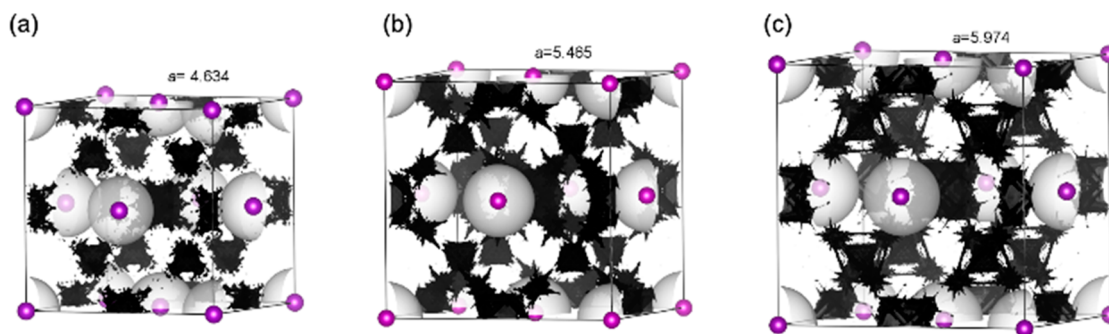
4. THE PRESSURE-OXIDATION EQUIVALENCE IN THE LIGHT OF THE CHEMICAL PRESSURE FORMALISM

4.1. Proving the Pressure-Oxidation Equivalence. Pressure-oxidation equivalence is based on empirical evidence showing that nonmetallic elements induce similar stress in the metallic sublattices where they are hosted as hydrostatic pressure does on the isolated metal structure.[21] As an example, the lattice parameter of fcc-Ca at 12 GPa is the same as the lattice parameter of the rock-salt CaO phase at zero pressure. Therefore, it can be understood that the effect of oxygen in the fcc-Ca sublattice of rock-salt CaO is equivalent to the mechanical compression shown by the metal structure at 12 GPa. If the pressure exerted by the nonmetal guest is high enough, the metal sublattice can eventually undergo a phase transition to a high-pressure structure, as in the case of the K_2S crystal previously discussed. Extending this view to cases where the metal sublattice is expanded would lead to consider the effect of the nonmetallic atom as that of a negative pressure.

To illustrate this apparent link between generalized stress and the redox state in a given structure under a broader perspective, we plot in Figure 6 the energy−volume equations
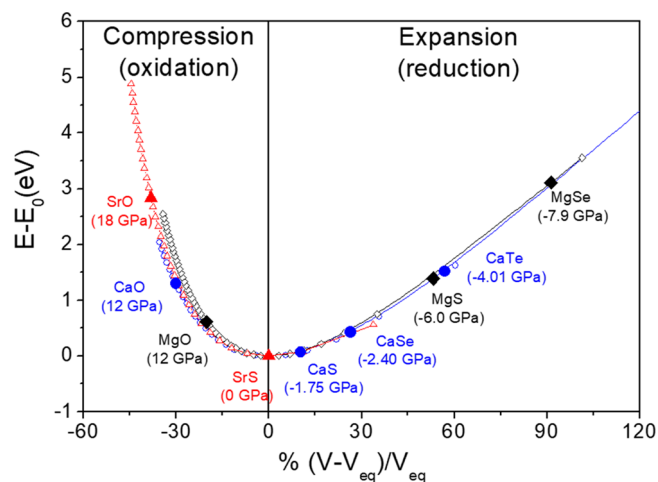

Figure 6. Energy−Volume equation of state curves for fcc-metallic Mg (black ◇), Ca (blue ○), and Sr (red △) along with the pressures associated with the volumes of the metallic sublattices in the corresponding MX (X = O, S, Se, Te) zero-pressure crystals. MgX (black ◆), CaX (blue ●), and SrX (red ▲).

of state of the fcc phases of Mg, Ca, and Sr metals emphasizing the pressures associated with the volumes of these lattices in

Figure 5. 3D CP analysis of the fcc-Na sublattices at the equilibrium volume of (a) NaF (CP = −0.044 au), (b) NaCl (CP = −0.021 au), and (c) NaBr (CP = −0.017 au). White isosurfaces are of CP = +0.001.

the rock-salt phases of MgX, CaX, and SrX (X: O, S, Se, and Te) crystals. Our calculated values are in good agreement with the available experimental data of ref 53. We assume that these pressures are induced in the metallic sublattices by the presence of the nonmetallic element. Whereas oxides are always in the repulsive part of the metal potential energy curves, thus indicating that the anion induces a compressive stress in the lattice, sulfides, selenides, and tellurides are always in the attractive regime, and therefore this fact could be viewed in these cases as a negative tensile stress (expansion) on the metallic lattice. Moreover, the expansion and contraction strains induced by the nonmetal guests seem to affect the different metallic lattices in an opposite direction. If we consider the oxygen anion, we can see how the compression effect increases from Mg to Sr; however, with the *expansive* anions the stretching behavior increases from Sr to Mg. These trends claim for the existence of a generalized pressure-oxidation correlation, which actually depends on the metal and the nonmetallic element.

Interestingly, similar trends are found when we analyze the evolution of the CP minima of the metallic lattices with volume. For instance, we display in Figure 7 how the CP
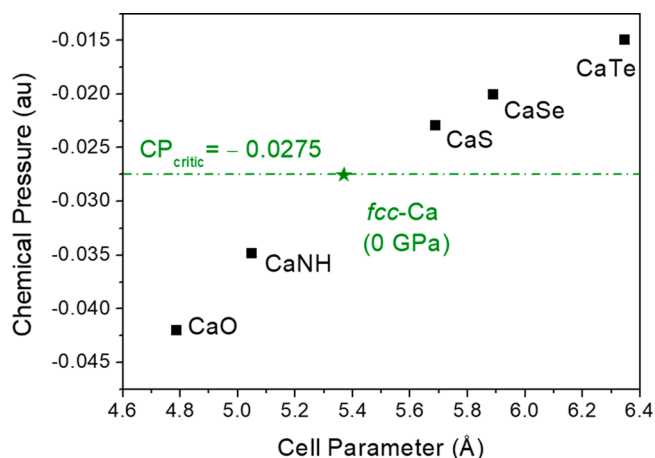
Figure 7. CP values at 4b (1/2, 1/2, 1/2) positions of metallic fcc-Ca at the different equilibrium lattice parameters of their corresponding CaX inorganic crystals (■). The green star represents the fcc-Ca CP value at zero pressure (reference value). Dash dotted line represents the critical chemical pressure, CP$_{critic}$, splitting the compressive (oxidation) and expansive (reduction) regimes.

minima found in the fcc-Ca structure increases monotonically with the lattice parameter. Using a simple Thomas-Fermi model, we can easily understand the obtained sublinear behavior. As in this framework the energy depends on the electron density to the 2/3 power, the CP (see eq [2]) should correlate with the lattice parameter as the power of −5, in fair agreement with the results displayed in Figure 7. The labels are located at the cell parameters of metallic fcc-Ca, where the equilibrium structures of their corresponding CaX compounds are found. Notice that the lowest minima CP values are obtained in the fcc-Ca structures with a reduced volume (positive-pressure regime induced by compressive guest elements), whereas the higher CP minima values correspond to expanded lattices (negative-pressure regime induced by expansive guest elements).

From this analysis, a critical value for the CP at the minima can be defined considering the value of the fcc-Ca metal at

zero pressure (CP$_{critic}$ = −0.0275). This value serves to define a boundary between nonmetallic elements inducing compression or expansion on the metallic lattice. Moreover, the observed trend points toward a relationship between the oxidation capacity of the nonmetallic element, the CP at the minima, and the pressure (positive or negative) exerted on the lattice. This connection supports us in using the CP formalism in what follows as a way to prove the equivalence between effective stress and the redox state.

Under the CP scheme, we can infer a correlation between these two quantities by analyzing the changes in the CP distribution in the unit cell of the fcc-Ca at zero pressure either by the application of external pressure or by the presence of nonmetallic elements leading to the rock-salt CaX phase. The comparison of the CP cross sections along the (001) plane of the rock-salt CaO structure (a = 4.829 Å) and the CP distributions of fcc-Ca at the same volume (p = 12 GPa) is shown in Figure 8. CP features around the Ca cores are mostly
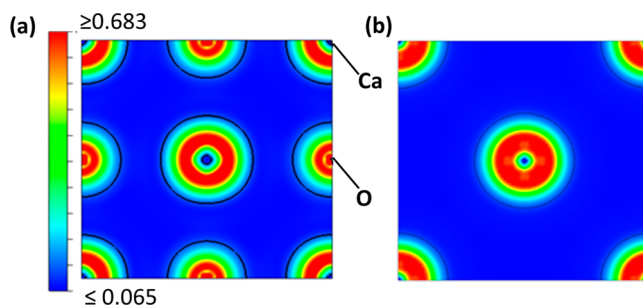
Figure 8. 2D CP cross sections along the (001) plane of (a) rock-salt CaO crystal and (b) fcc-Ca at the same lattice parameter than the rock-salt CaO. Black lines correspond to the CP = 0 isoline. Pressures are given in atomic units.

maintained, reflecting that the core−shell structure is essentially preserved during the electron density reorganization induced by pressure or by oxidation. Negative CP values out of the core positions are also very similar in both Figure 8a,b, except, of course, at the positions where oxygen atoms are located.

A more detailed analysis is provided in Figure 9 from the plot of the one-dimensional (1D) CP profiles along the Ca−Ca path in the fcc-Ca lattices at 0 and 12 GPa, and at zero pressure in the rock-salt CaO phase. It can be seen that both pressure and oxidation increase the CP maxima located at the core region from +0.6028 au in the zero-pressure metallic Ca to +0.7125 and +0.8571 au, respectively. This effect is accompanied by a lowering of the negative CP along the intermediate region of the interatomic path. Consequently, both positive pressure and oxidation lead to similar CP features in the core region and in the interstices. Therefore, CP indicates that electron density accumulation produced by the oxidation is also produced by the compression of the lattice in the line of the claimed pressure oxidation equivalence. Nonetheless the slight differences in the CP values reflect that such an effect is similar but not equal. Such differences can be attributed to the fact that, in the oxide Ca, atoms formally transfer two electrons to O forming Ca^{2+} and O^{2-} ions, whereas in the case of fcc-Ca at 12 GPa such an electron transfer is not formally produced, at least to the same extend, because valence electrons are partially delocalized.
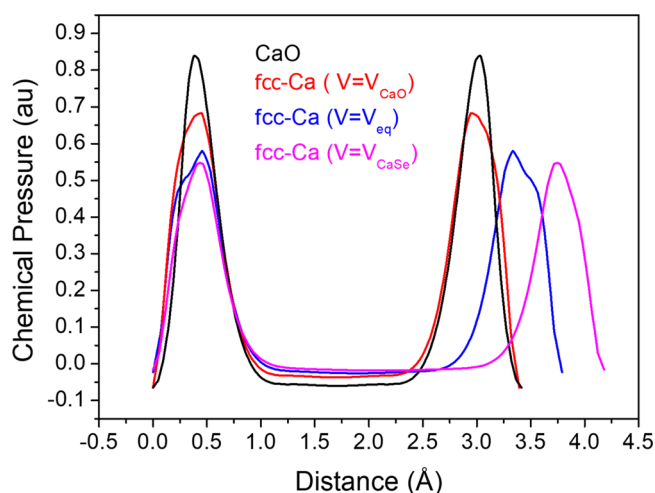
Figure 9. 1D Ca−Ca CP profiles of metallic fcc-Ca at its equilibrium volume (blue line), metallic fcc-Ca at the equilibrium volume of the rock-salt CaO crystal (red line), metallic fcc-Ca at the equilibrium volume of the rock-salt CaSe crystal (magenta line), and within the rock-salt CaO crystal at its equilibrium volume (black line).

When compared with the 1D Ca−Ca profile in fcc-Ca at the same volume of the CaSe equilibrium structure ($p = -2.40$ GPa), an opposite effect is observed. A reduction of the CP values at the core regions and an increase at the interstitial voids are produced. As a result, the pressure-oxidation state principle seems to hold again. However, in this case this behavior is associated with a depletion (reduction) of the electron density at the interstices toward the nuclei positions due to the expansion of the lattice induced either by the nonmetallic atom or the (negative) pressure.

4.2. Linking Pressure and Oxidation through Atomic Electronegativity. So far we demonstrated that metal oxidation induced by nonmetallic atoms and hydrostatic pressure lead to similar structural effects. Our ultimate goal is to seek for a chemical basis for this correlation. Traditionally, size effects have been invoked to explain the compressive or expansive behavior of the metallic sublattices in inorganic compounds.[7,8] We can apply this idea using Shannon radii[60] for O, S, Se, and Te (1.40, 1.84, 1.98, and 2.21 Å, respectively) and the metallic radii of fcc Mg, Ca, and Sr (1.60, 2.00, and 2.15 Å, respectively). For instance, on the one hand, considering CaX compounds as a test, an increase in the lattice parameter is predicted along the O, S, Se, and Te series, following the same trend as the ionic radii. On the other hand, only the Ca sublattice in CaTe should suffer an expansion effect, since Te radius is the only one greater than that of Ca in the fcc structure at equilibrium. However, this is not the observed result, as demonstrated in Figures 6 and 7, where the Ca sublattice in CaS and CaSe is also observed to show a larger lattice parameter than in fcc-Ca. Similar flaws of this purely geometric reasoning are also found for the Mg and Sr series.

Analogously, the amount of charge density transferred from the metallic atoms to the guest elements could also be used as a means to throw light into the pressure-oxidation correlation, since cation/anion charges can inform on the oxidation strength of the nonmetallic element. By means of the Atoms in Molecules formalism, we calculated the following Bader charges for Ca in CaO, CaS, CaSe, and CaTe: 1.445, 1.423, 1.395, and 1.374, respectively. As expected, such a decrease in the charge of Ca correlates with a decrease in the oxidation

power of the guest element and also with an increase in the lattice parameter. However, nothing can be inferred regarding the contraction/expansion observed in the zero pressure pure metallic Ca lattice upon crystal formation. In the case of a pure metal, Bader charges are always zero regardless the pressure (or volume) applied on the unit cell. In this sense, all the guest elements formally oxidize the submetal lattice, and therefore, it is not possible to prove if pressure regulates the amount of charge accumulated in the interstice voids of the pure metal.

Consequently, we have to recall to further elaborated arguments to explain both the expansive and compressive regimes. For this, we will again invoke the Vegas' hypothesis[15] on the equivalence between oxidation and pressure at the microscopic level, based on the fact that pressure induces an accumulation of electron density in the interstices of the metallic lattice. This is in concordance with the emergence of non-nuclear maxima[61] and the existence of electrides at high pressure.[18−20] According to this view, when the nonmetallic element is hosted just at the same positions in an unstressed metal, a similar effect on the electron density of the metal is expected. Whereas this result seems to hold in the compressive regime, this rule must be carefully applied when the metal subarray suffers an expansion induced by the nonmetallic atom. In such cases, the increased metal−metal interatomic distances lead to a reduction of the electron density in the voids, which may be regarded as somewhat contradictory from the perspective of an *oxidation* process. Furthermore, according to the free electron model,[48,49] metallic atoms transfer its valence electrons to the lattice interstices acquiring formally an oxidized state already in the zero-pressure metallic phase.

This view can be quantitatively confirmed through the evaluation of the number of core electrons of the metal at different pressure (volume) conditions. As we saw in the previous sections, the CP = 0 contour in metallic Ca defines a boundary between the positive CP zone representing a sphere corelike region and the negative-pressure background associated with the delocalized sea of electrons (see, e.g., Figure 1a). A measure of the number of core electrons (n_e), and therefore an estimation of the amount of charge transferred to the metal voids, can be given by integrating the electron density within this positive chemical pressure region. Values are collected in Table 1, where we selected the zero-pressure metallic phase as our reference within the AMM model for the ongoing discussion.

Indeed, when we compared the number of corelike electrons in the pure fcc-Ca metal at the zero-pressure equilibrium

Table 1. Lattice Parameters (a), Pressures (p), Radii (R_{core}), and Number of Electrons (n_e) of the Corelike Region of fcc-Ca at Its Zero Pressure Equilibrium Volume and at the Corresponding Volumes of Different CaX Compounds (X = O, S, Se, Te)[a]

	a (Å)	p (GPa)	R_{core} (Å)	n_e	Δn_e
fcc-Ca (V_{CaO})	4.787	12	0.955	7.181	−0.216
fcc-Ca (V_{eq})	5.410	0	1.007	7.397	0
fcc-Ca (V_{CaS})	5.689	−1.75	1.043	7.520	0.123
fcc-Ca (V_{CaSe})	5.916	−2.40	1.065	7.585	0.188
fcc-Ca (V_{CaTe})	6.348	−4.01	1.119	7.714	0.317

[a]Δn_e stands for the difference between the number of electrons in the corelike region of fcc-Ca at different pressures with respect to the zero-pressure value.

583 volume with those corresponding to the volumes of their CaX
584 compounds (see Table 1), then the generalized stress-redox
585 relationship is clearly illustrated. For instance, in the case of
586 Ca, an estimation of the redox effect induced in the pure
587 metallic lattice as a consequence of the structural distortions
588 associated with the guest elements (O, S, Se Te) is given by
589 the number of corelike electrons transferred Δn_e. The latter
590 quantity is calculated as the difference between the number of
591 corelike electrons of the pure metal Ca metal at the volumes of
592 the respective CaX compounds and the value of pure Ca metal
593 at zero pressure (see Table 1). In the case of O atom, it exerts
594 a pressure of 12 GPa on the lattice, which induces a core
595 electron transfer of −0.215 to the interstitial voids producing
596 an oxidation effect in the metallic lattice. On the contrary, the
597 expansion effect induced by S, Se, and Te exerts −1.75, −2.40,
598 and −4.01 GPa on the submetal lattice, which corresponds to
599 an electron core increase of 0.123, 0.193, and 0.317 au,
600 respectively. Such an increase in the number of core electrons
601 clearly manifests that S, Se, and Te induce a reduction effect on
602 the lattice (previous to the oxidation produced by the
603 formation of their respective anions). In summary, although
604 in the global process the metal is formally oxidized, if we take
605 the zero-pressure metal as a reference state, we can distinguish
606 nonmetallic atoms behaving either as oxidizing or reducing
607 agents. These redox processes are unequivocally manifested
608 through the volume change of the metal sublattice providing
609 further support to the pressure-oxidation equivalence, which
610 should be more appropriately renamed as general stress-redox
611 correspondence, as we advanced in the previous section.
612   The fundamental basis behind this general stress-redox
613 equivalence is provided by the Pearson-Parr's electronegativity
614 equalization principle.[37,38] This principle explains not only the
615 failure of the radius ratio rule but also the observed
616 contraction−expansion trends. Accordingly, the electron
617 density transferred from the metallic atoms to the guest
618 element should correlate with the difference between the
619 electronegativity of the nonmetallic element and the capacity
620 of the metal to donate electron charge to the anion position.
621 The latter can be either quantified by the value of the CP at the
622 minima located at that 4b position, as we saw in the previous
623 sections, or by the number of core electrons transferred Δn_e.
624   Since both quantities increase (decrease) monotonically
625 with the volume (pressure) of the metal phase, we can
626 understand that the metal array fits its lattice parameter to
627 fulfill the equalization principle. If this lattice parameter is
628 fixed, then only nonmetallic elements within a narrow range of
629 electronegativity values could be hosted by the metallic lattice.
630 Under the equalization principle scheme, this electronegativity
631 range would ideally be a narrow one with just the value that
632 perfectly matches the metal capability to accumulate electron
633 density at the anion position, which we demonstrated that can
634 be quantitatively associated with the CP minimum value and/
635 or the number of the core electrons transferred.
636   This view is confirmed when we plot the CP values at the 4b
637 positions and Δn_e of the fcc-Ca structure using the volumes of
638 the respective CaX compounds (X: O, S, Se, Te) with respect
639 to the Pauling electronegativity of the different X atoms (see
640 Figure 10). The linear correlations observed in Figure 10 seem
641 to be quite general and support the generalized stress-redox
642 correlation as a general principle. Following a referee
643 recommendation, we would like to be very clear at this
644 respect. By "quite general" we mean that this type of linear
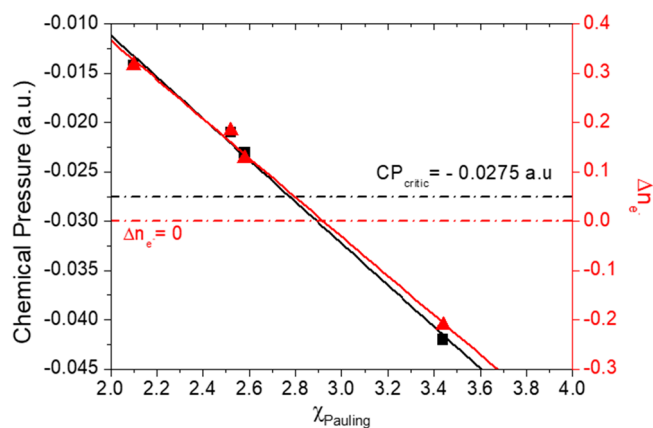645 trend also holds in other metals. For example, in the ones

Figure 10. Metallic fcc-Ca CP values at the 4b position (■) and number of corelike electrons transferred Δn_e (▲) for the different CaX (X = O, S, Se, Te) compounds against the Pauling electronegativity of the corresponding X atom. Black and red straight lines correspond, respectively, to the linear fittings of the CP data, CP $= 0.0311 - 0.0211 \cdot \chi_{Pauling}$, and Δn_e data, $\Delta n_e = 1.164 - 0.0398 \cdot \chi_{Pauling}$.

646 explored in this work (see, e.g., the plots for Na and Mg
647 collected in the Supporting Information file) linear fittings of
648 similar quality were obtained. It should be also pointed out
649 that CP-χ values obviously depend on the metal and the
650 particular structure, since the reference redox state varies from
651 lattice to lattice. As a corollary, we can state that the Pearson-
652 Parr's equalization principle is the driving force expanding or
653 compressing the metal structure to equalize the electro-
654 negativity of the guest element with the CP at the metal voids
655 (or equivalently its charge), leading the formation of the
656 inorganic crystal.
657   From the plot of Figure 10, a quite high value of 2.78 is
658 obtained for the electronegativity of the zero pressure fcc-Ca
659 lattice acting on the 4b position. Such a value does not
660 represent the actual electronegativity of *isolated* Ca but a local
661 value, which evidences that voids are preferred positions of the
662 structure where formally the metal electron density is
663 accumulated.
664   Interestingly enough, this linear trend also provides a way to
665 infer either the electronegativity of the nonmetallic atom
666 (group) located at the Ca 4b position or, alternatively, the
667 equilibrium lattice parameter of an unknown CaX compound.
668 For instance, in the case of the CaNH crystal we propose a
669 Pauling electronegativity value for the NH group of 3.11 based
670 on its lattice parameter of 5.05 Å. Using this value of
671 electronegativity for the NH group, we can now estimate the
672 lattice parameter of the hypothetical rock-salt MgNH
673 compound by means of the CP-lattice parameter correlation
674 of Mg depicted in Figures S4 and S5 of Supporting
675 Information. A value of 4.18 Å is obtained, which is not too
676 far from the value of 4.35 Å derived for a cubic lattice assuming
677 the same volume as the experimental zero pressure value
678 determined for the hexagonal MgNH phase.[62] This result
679 points to the transferability between the guest electro-
680 negativities obtained in this work but also highlights the
681 potential of the chemical pressure to anticipate lattice
682 parameters of unknown phases. Obviously, this feature has
683 nothing to do with the possible determination of the stable
684 phase of the compound at given *p, T* conditions (that requires
685 the evaluation of the Gibbs energy), which up to now is in
686 general far to be foreseen under the CP-AMM scheme.

As negative CP and atom electronegativity represent the capability of the electron density to be accumulated, respectively, in the metal voids and in the nonmetallic atom, compressive effects will result when the atom capability is higher than that of the corresponding metal, whereas expansive effects will result from an excess of the electron density in the metal voids compared to one that the nonmetallic atom can attract. From another perspective, such a capability can be interpreted as the oxidation potential. Therefore, on the one hand, if the guest atom has a higher oxidation potential than the corresponding metal, a compressive effect (positive pressure) must be applied to equalize its capability. On the other hand, in the case of a lower oxidation potential, the metal must *move* to the negative-pressure regime (expansion) to reach the oxidation state of the anion.

Finally, as the CP formalism allows us to decompose chemical pressure into different meaningful contributions,[28] it is interesting to evaluate the contribution coming from the potential energy term, which is described in the CP program as the local pseudopotential (PSP) contribution. This is mainly responsible for the nucleus−electron interaction, and so it is connected to the tendency of a given unit cell position to attract the electron density, which we ultimately associate with the total electronegativity at that point.

In Table 2, we collected the total CP and the potential energy CP contribution at the 4b positons of fcc-Ca at

Table 2. Total CP and Potential CP Contribution at the 4b Position of the Metallic fcc-Ca Structure at Different Pressures Corresponding to the Equilibrium Volumes of CaX (X = O, S, Se, Te) Compounds[a]

	a (Å)	p (GPa)	CP(4b) (au)	$CP_{Potential}$(4b) (au)
fcc-Ca (V_{CaO})	4.787	12	−0.042 12	−0.061 89
fcc-Ca (V_{eq})	5.410	0	−0.040 59	−0.040 58
fcc-Ca (V_{CaS})	5.689	− 1.75	−0.034 15	−0.034 10
fcc-Ca (V_{CaSe})	5.916	− 2.40	−0.031 01	−0.031 01
fcc-Ca (V_{CaTe})	6.348	− 4.01	−0.020 91	−0.020 82

[a]The CP value at zero pressure is included for reference.

pressures corresponding to the equilibrium volumes of different CaX (X = O, S, Se, Te) compounds. The potential energy pressure is by far mainly responsible for the overall negative pressure at such positions indicating that electronegativity dominates the guest insertion on the lattice. Furthermore, the more the pressure is applied on the structure the more is the potential contribution in absolute value. To further illustrate this behavior, we plotted in Figure 11 the potential energy contribution to CP (CP_{Pot}) against the number of core electrons transferred Δn_e for fcc-Ca at the different volumes of the CaX compounds. As we have previously seen, Δn_e represents the amount of charge transferred from the Ca cores to the interstitial voids and, therefore, in analogy with Bader charges in ionic compounds, can be used as an estimation of the electronegativity changes in the metal. Interestingly, a linear trend between potential energy CP and Δn_e is observed, thus evidencing that the increase of the potential energy CP (in absolute value) is ultimately related to the decreasing of the electronegativity of the metal, in total concordance with the clarifying analysis of a recent publication of Rahm et al.[55] Furthermore, such a result leads us to propose that the expansion and the contraction of the unit cell are intrinsic mechanisms of the metal lattice to regulate its
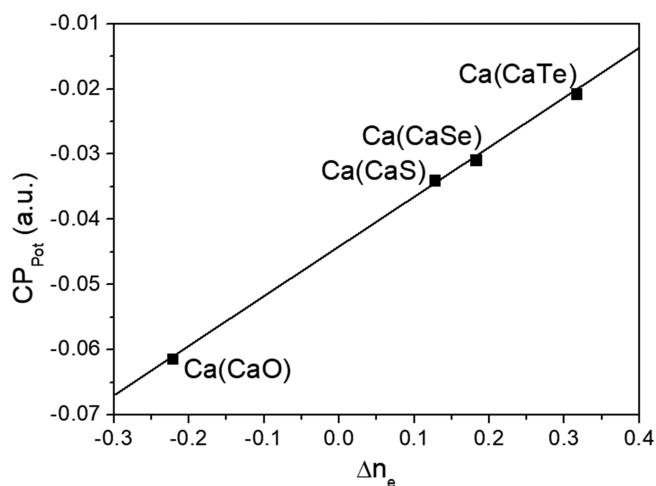

Figure 11. Potential energy contribution to CP (CP_{Pot}) against the number of core electrons transferred Δn_e for fcc-Ca at the different volumes of the CaX compounds.

potential energy pressure and therefore its local electronegativity at the relevant interstitial positions.

CONCLUSIONS

Throughout this Manuscript, we have tried to take some steps forward in the understanding of inorganic crystalline structures. First, the DFT-CP approach has proved to be an efficient verifier of the premises of the AMM model. Minima of CP are clearly identified in a collection of metallic structures just at the precise positions where nonmetallic elements are situated in the corresponding inorganic crystalline compounds. Second, the pressure-oxidation equivalence inherent to the AMM model has been explained and consequently generalized finding a robust support in the Pearson-Parr's electronegativity equalization principle. Our results provide a clear conclusion on the structures of inorganic crystals. Ionic compounds are formed through the distortion of their underlying metal sublattice in such a way that the metallic structure adjusts its volume leading a value for the potential energy chemical pressure (local electronegativity) at the relevant interstice positions to formally host the nonmetallic element with the *same* electronegativity. As far as we know, this is the first time that a clear connection between a local electronegativity acting on a specific position of a metal lattice is correlated to the formation of the corresponding ionic compound.

ASSOCIATED CONTENT

S **Supporting Information**

The Supporting Information is available free of charge on the ACS Publications website at DOI: 10.1021/acs.inorg-chem.9b01470.

Computational details, fcc-Mg and sc-Mg CP analysis, and Na and Mg CP-electronegativity correlations (PDF)

AUTHOR INFORMATION

Corresponding Authors

*E-mail: jmrecio@uniovi.es. (J.M.R.)
*E-mail: hokashif@science.helwan.edu.eg. (H.H.O.)

ORCID

Hussien H. Osman: 0000-0003-1411-8299
J. Manuel Recio: 0000-0002-3182-7508

Author Contributions

The manuscript was written through contributions of all authors. All authors have given approval to the final version of the manuscript.

Notes

The authors declare no competing financial interest.

■ REFERENCES

(1) Pauling, L. *The Nature of the Chemical Bond and the Structure of Molecules and Crystals: An Introduction to Modern Structural Chemistry*; 3rd ed.; Cornell University Press, 1960.

(2) Gatti, C. Chemical bonding in crystals: new directions. *Z. Kristallogr. - Cryst. Mater.* **2005**, *220*, 399−457.

(3) Weinhold, F.; Landis, C. R. *Valency and Bonding: A Natural Bond Orbital Donor-acceptor Perspective*; Cambridge University Press: Cambridge, UK, 2005.

(4) Frenking, G.; Shaik, S. *The Chemical Bond: Fundamental Aspects of Chemical Bonding*; Wiley VCH: Weinheim, Germany, 2014; Vol. *1*.

(5) Schmidt, M. W.; Ivanic, J.; Ruedenberg, K. The Physical Origin of Covalent Bonding. In *The Chemical Bond. Fundamental Aspects of Chemical Bonding*; Wiley-VCH Verlag: Weinheim, Germany, 2014; Chapter 1.

(6) Lewis, G. N. *Valence and the structure of atoms and molecules*; Dover: New York, 1966.

(7) Pauling, L. The Principles Determining the Structure of Complex Ionic Crystals. *J. Am. Chem. Soc.* **1929**, *51* (4), 1010−1026.

(8) Pauling, L. *The Nature of the Chemical Bond*; Cornell University Press: Ithaca, NY, 1939.

(9) O'Keeffe, M.; Hyde, B. G. An alternative approach to non-molecular crystal structures with emphasis on the arrangements of cations. In *Cation Ordering and Electron transfer*; Springer: Berlin, Germany, 1985; Vol. *61*, pp 77−144.

(10) O'Keeffe, M.; Hyde, B. G. The Role of Nonbonded Forces in Crystals. In *Structure and Bonding in Crystals*; Academic Press: New York, 1981; Vol. *1*, pp 227−253.

(11) Von Schnering, H. G.; Nesper, R. How Nature Adapts Chemical Structures to Curved Surfaces. *Angew. Chem., Int. Ed. Engl.* **1987**, *26*, 1059−1080.

(12) Schubert, K. *Kristallstrukturen Zweikomponentiger Phasen*; Springer-Verlag: Berlin, Germany, 1964; Chapter 2.

(13) Vegas, A.; Martínez-Cruz, L. A. A study of cation arrays in MB2, MB4 and MB6 borides. Part II. Cluster formation and bonding aspects. *Z. Kristallogr. - Cryst. Mater.* **1995**, *210*, 581−584.

(14) Vegas, Á.; Jansen, M. Structural relationships between cations and alloys: an equivalence between oxidation and pressure. *Acta Crystallogr., Sect. B: Struct. Sci.* **2002**, *B58*, 38−51.

(15) Vegas, Á.; Santamaría-Pérez, D.; Marqués, M.; Flórez, M.; Garcia Baonza, V.; Recio, J. M. Anions in metallic matrices model: application to the aluminium crystal chemistry. *Acta Crystallogr., Sect. B: Struct. Sci.* **2006**, *62*, 220−227.

(16) Marqués, M.; Florez, M.; Recio, J. M.; Santamaría, D.; Vegas, A.; Garcia Baonza, V. Structure, Metastability, and Electron Density of Al Lattices in Light of the Model of Anions in Metallic Matrices. *J. Phys. Chem. B* **2006**, *110*, 18609−18618.

(17) Mori-Sánchez, P.; Pendás, Á. M.; Luaña, V. Polarity inversion in the electron density of BP crystal. *Phys. Rev. B: Condens. Matter Mater. Phys.* **2001**, *63*, 125103−1.

(18) Marqués, M.; Ackland, G. J.; Lundegaard, L. F.; Stinton, G.; Nelmes, R. J.; McMahon, M. I.; Contreras-García, J. Potassium under Pressure: A Pseudobinary Ionic Compound. *Phys. Rev. Lett.* **2009**, *103*, 115501−115505.

(19) Miao, M. M.; Hoffmann, R. High Pressure Electrides: A Predictive Chemical and Physical Theory. *Acc. Chem. Res.* **2014**, *47*, 1311−1317.

(20) Miao, M. M.; Hoffmann. High Pressure Electrides: the Chemical Nature of Interstitial Quasi-atoms. *J. Am. Chem. Soc.* **2015**, *137*, 3631−3637.

(21) Vegas, Á.; Mattesini, M. Towards a generalized vision of oxides: disclosing the role of cations and anions in determining unit-cell dimensions. *Acta Crystallogr., Sect. B: Struct. Sci.* **2010**, *B66*, 338−344.

(22) Vegas, Á. Concurrent Pathways in the Phase Transitions of Alloys and Oxides: Towards an Unified Vision of Inorganic Solids. *Struct. Bonding (Berlin, Ger.)* **2011**, *138*, 133−198.

(23) Martínez-Cruz, L. A.; Ramos-Gallardo, Á.; Vegas, Á. MSn and MSnO3 (M = Ca, Sr, Ba): New Examples of Oxygen-Stuffed Alloys. *J. Solid State Chem.* **1994**, *110*, 397−398.

(24) Filippetti, A.; Fiorentini, V. Theory and applications of the stress density. *Phys. Rev. B: Condens. Matter Mater. Phys.* **2000**, *61*, 8433−8442.

(25) Rogers, C. L.; Rappe, A. M. Geometric formulation of quantum stress fields. *Phys. Rev. B: Condens. Matter Mater. Phys.* **2002**, *65*, 224117.

(26) Godfrey, M. J. Stress field in quantum systems. *Phys. Rev. B: Condens. Matter Mater. Phys.* **1988**, *37*, 10176−10183.

(27) Nielsen, O. H.; Martin, R. M. Quantum-mechanical theory of stress and force. *Phys. Rev. B: Condens. Matter Mater. Phys.* **1985**, *32*, 3780−3791.

(28) Ziesche, P.; Gräfenstein, J.; Nielsen, O. H. Quantum-mechanical stress and a generalized virial theorem for clusters and solids. *Phys. Rev. B: Condens. Matter Mater. Phys.* **1988**, *37*, 8167−8178.

(29) Fredrickson, D. C. DFT-Chemical Pressure Analysis: Visualizing the Role of Atomic Size in Shaping the Structures of Inorganic Materials. *J. Am. Chem. Soc.* **2012**, *134*, 5991−5999.

(30) Osman, H. H.; Salvadó, M. A.; Pertierra, P.; Engelkemier, J.; Fredrickson, D. C.; Recio, J. M. Chemical Pressure Maps of Molecules and Materials: Merging the Visual and Physical in Bonding Analysis. *J. Chem. Theory Comput.* **2018**, *14*, 104−114.

(31) Osman, H. H.; Andrés, J.; Salvadó, M. A.; Recio, J. M. Chemical Bond Formation and Rupture Processes: An Application of DFT-Chemical Pressure Approach. *J. Phys. Chem. C* **2018**, *122*, 21216−21225.

(32) Fredrickson, D. C. Electronic Packing Frustration in Complex Intermetallic Structures: The Role of Chemical Pressure in Ca2Ag7. *J. Am. Chem. Soc.* **2011**, *133*, 10070−10073.

(33) Berns, M. V.; Fredrickson, D. C. Structural Plasticity: How Intermetallics Deform Themselves in Response to Chemical Pressure, and the Complex Structures That Result. *Inorg. Chem.* **2014**, *53*, 10762−10771.

(34) Engelkemier, J.; Berns, V. M.; Fredrickson, D. C. First-Principles Elucidation of Atomic Size Effects Using DFT-Chemical Pressure Analysis: Origins of Ca36Sn23's Long-Period Superstructure. *J. Chem. Theory Comput.* **2013**, *9*, 3170−3180.

(35) Engelkemier, J.; Fredrickson, D. C. Chemical Pressure Schemes for the Prediction of Soft Phonon Modes: A Chemist's Guide to the Vibrations of Solid State Materials. *Chem. Mater.* **2016**, *28*, 3171−3183.

(36) Chattaraj, P. K.; Lee, H.; Parr, R. G. HSAB Principle. *J. Am. Chem. Soc.* **1991**, *113*, 1855−1856.

(37) Pearson, R. G. Absolute Electronegativity and Hardness: Application to Inorganic Chemistry. *Inorg. Chem.* **1988**, *27*, 734−740.

(38) Parr, R. G.; Pearson, R. G. Absolute Hardness: Companion Parameter to Absolute Electronegativity. *J. Am. Chem. Soc.* **1983**, *105*, 7512−7516.

(39) Goedecker, S.; Teter, M.; Hutter, J. Separable Dual-space Gaussian Pseudopotentials. *Phys. Rev. B: Condens. Matter Mater. Phys.* **1996**, *54*, 1703−1710.

(40) Hartwigsen, C.; Goedecker, S.; Hutter, J. Relativistic Separable Dual-space Gaussian Pseudopotentials from H to Rn. *Phys. Rev. B: Condens. Matter Mater. Phys.* **1998**, *58*, 3641−3662.

(41) Gonze, X.; Jollet, F.; Abreu Araujo, F.; Adams, D.; Amadon, B.; Applencourt, T.; Audouze, C.; Beuken, J. M.; Bieder, J.; Bokhanchuk, A.; Bousquet, E.; Bruneval, F.; Caliste, D.; Côté, M.; Dahm, F.; Da Pieve, F.; Delaveau, M.; Di Gennaro, M.; Dorado, B.; Espejo, C.; Geneste, G.; Genovese, L.; Gerossier, A.; Giantomassi, M.; Gillet, Y.; Hamann, D. R.; He, L.; Jomard, G.; Laflamme Janssen, J.; Le Roux, S.; Levitt, A.; Lherbier, A.; Liu, F.; Lukačević, I.; Martin, A.; Martins, C.; Oliveira, M. J T.; Poncé, S.; Pouillon, Y.; Rangel, T.; Rignanese, G. M.; Romero, A. H.; Rousseau, B.; Rubel, O.; Shukri, A. A.; Stankovski, M.; Torrent, M.; Van Setten, M. J.; Van Troeye, B.; Verstraete, M. J.; Waroquiers, D.; Wiktor, J.; Xu, B.; Zhou, A.; Zwanziger, J. W. Recent developments in the ABINIT software package. *Comput. Phys. Commun.* **2016**, *205*, 106−131.

(42) Gonze, X.; Amadon, B.; Anglade, P.-M.; Beuken, J.-M.; Bottin, F.; Boulanger, P.; Bruneval, F.; Caliste, D.; Caracas, R.; Côté, M.; Deutsch, T.; Genovese, L.; Ghosez, P.; Giantomassi, M.; Goedecker, S.; Hamann, D. R.; Hermet, P.; Jollet, F.; Jomard, G.; Leroux, S.; Mancini, M.; Mazevet, S.; Oliveira, M. J. T.; Onida, G.; Pouillon, Y.; Rangel, T.; Rignanese, G.-M.; Sangalli, D.; Shaltaf, R.; Torrent, M.; Verstraete, M. J.; Zerah, G.; Zwanziger, J. W. ABINIT: First-principles Approach to Material and Nanosystem Properties. *Comput. Phys. Commun.* **2009**, *180*, 2582−2615.

(43) Gonze, X.; Rignanese, G.-m.; Verstraete, M.; Beuken, J.-m.; Pouillon, Y.; Caracas, R.; Raty, J.-y.; Olevano, V.; Bruneval, F.; Reining, L.; Godby, R.; Onida, G.; Hamann, D. R.; Allan, D. C. A Brief Introduction to the ABINIT Software Package. *Z. Kristallogr. - Cryst. Mater.* **2005**, *220*, 558−562.

(44) Monkhorst, H.; Pack, J. Special Points for Brillouin-zone Integrations. *J. Phys. Rev. B* **1976**, *13*, 5188−5192.

(45) Hilleke, K. P.; Fredrickson, D. C. Discerning Chemical Pressure amidst Weak Potentials: Vibrational Modes and Dumbbell/Atom Substitution in Intermetallic Aluminides. *J. Phys. Chem. A* **2018**, *122*, 8412−8426.

(46) Momma, K.; Izumi, F. VESTA 3 for Three-dimensional Visualization of Crystal, Volumetric and Morphology data. *J. Appl. Crystallogr.* **2011**, *44*, 1272−1276.

(47) Bader, R. F. Atoms in Molecules. *Acc. Chem. Res.* **1985**, *18*, 9−15.

(48) Otero de la Roza, A.; Johnson, E. R.; Luaña, V. Critic2: A program for real-space analysis of quantum chemical interactions in solids. *Comput. Phys. Commun.* **2014**, *185*, 1007−101.

(49) Yu, M.; Trinkle, D. R. Accurate and efficient algorithm for Bader charge integration. *J. Chem. Phys.* **2011**, *134*, 064111−1−8.

(50) Vegas, Á. *Structural Models of Inorganic Crystals*, 1st ed.; Universitat Politècnica de València, 2018.

(51) Drude, P. Zur Elektronentheorie der Metalle. *Ann. Phys.* **1900**, *306*, 566−613.

(52) Sommerfeld, A. Zur Elektronentheorie der Metalle auf Grund der Fermischen Statistik. *Eur. Phys. J. A* **1928**, *47*, 1−32.

(53) Anzellini, S.; Errandonea, D.; MacLeod, S. G.; Botella, P.; Daisenberger, D.; De'Ath, J. M.; Gonzalez-Platas, J.; Ibáñez, J.; McMahon, M. I.; Munro, K. A.; Popescu, C.; Ruiz-Fuertes, J.; Wilson, C. W. Phase diagram of calcium at high pressure and high temperature. *Phys. Rev. Materials* **2018**, *2*, 083608−1−8.

(54) Errandonea, D.; Boehler, R.; Ross, M. Melting of the alkaline-earth metals to 80 GPa. *Phys. Rev. B: Condens. Matter Mater. Phys.* **2001**, *65*, 012108−1−4.

(55) Rahm, M.; Cammi, R.; Ashcroft, N. W.; Hoffmann, R. Squeezing All Elements in the Periodic Table: Electron Configuration and Electronegativity of the Atoms under Compression. *J. Am. Chem. Soc.* **2019**, *141*, 10253−10271.

(56) Beck, H. P.; Lederer, G. Thermische Dilatation und Hochdruckverhalten der Zintl-Phasen CaSn und BaSn. *Z. Anorg. Allg. Chem.* **1993**, *619*, 897−900.

(57) Vegas, Á.; Grzechnik, A.; Hanfland, M.; Mühle, C.; Jansen, M. Antifluorite to Ni$_2$In-type phase transition in K$_2$S at high pressures. *Solid State Sci.* **2002**, *4*, 1077−1081.

(58) Megchiche, E. H.; Amarouche, M.; Mijoule, C. First-principles calculations of the diffusion of atomic oxygen in nickel: thermal expansion contribution. *J. Phys.: Condens. Matter* **2007**, *19*, 296201−299216.

(59) Kim, J.; Shin, S. H.; Jung, J. A.; Choi, K. J.; Kim, J. H. First-principles study of interstitial diffusion of oxygen in nickel chromium binary alloy. *Appl. Phys. Lett.* **2012**, *100*, 131904−131912.

(60) Shannon, R. D. Revised Effective Ionic Radii and Systematic Studies of Interatomic Distances in Halides and Chalcogenides. *Acta Crystallogr., Sect. A: Cryst. Phys., Diffr., Theor. Gen. Crystallogr.* **1976**, *32*, 751−767.

(61) Pendás, A.; Blanco, M. A.; Costales, A.; Sánchez, P.; Luaña, V. Non-nuclear Maxima of the Electron Density. *Phys. Rev. Lett.* **1999**, *83*, 1930.

(62) Dolci, F.; Napolitano, E.; Weidner, E.; Enzo, S.; Moretto, P.; Brunelli, M.; Hansen, T.; Fichtner, M.; Lohstroh, W. Magnesium Imide: Synthesis and Structure Determination of an Unconventional Alkaline Earth Imide from Decomposition of Magnesium Amide. *Inorg. Chem.* **2011**, *50* (3), 1116−1122.